Artificial Intelligence in Agriculture 6 (2022) 90–99

Contents lists available at ScienceDirect

Artificial Intelligence in Agriculture

journal homepage: http://www.keaipublishing.com/en/journals/artificial-intelligence-in-agriculture/

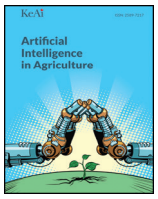

Analysis of land surface temperature using Geospatial technologies in Gida Kiremu, Limu, and Amuru District, Western Ethiopia

Mitiku Badasa Moisa [a,*], Bacha Temesgen Gabissa [b], Lachisa Busha Hinkosa [a], Indale Niguse Dejene [c], Dessalegn Obsi Gemeda [d]

[a] Department of Agricultural Engineering, Faculty of Technology, Wollega University Shambu campus, Shambu, Ethiopia
[b] Department of Fisheries and Aquatic Sciences, Faculty of Agriculture, Wollega University Shambu campus, Shambu, Ethiopia
[c] Department of Earth Sciences, College of Natural and Computational Sciences, Wollega University Nekemte Campus, Nekemte, Ethiopia
[d] Department of Natural Resource Management, College of Agriculture and Veterinary Medicine, Jimma University, Jimma, Ethiopia

ARTICLE INFO

Article history:
Received 22 February 2022
Received in revised form 26 May 2022
Accepted 20 June 2022
Available online 23 June 2022

Keywords:
LST
NDVI
NDBaI
MNDWI
Satellite data

ABSTRACT

Degradation of vegetation cover and expansion of barren land are remained the leading environmental problem at global level. Land surface temperature (LST), Normalized Difference Vegetation Index (NDVI), Normalized Difference Barren Index (NDBaI), and Modified Normalized Difference Water Index (MNDWI) were used to quantify the changing relationships using correlation analysis. This study attempted to analyze the relationship between LST and NDVI, NDBaI, and MNDWI using Geospatial technologies in Gida Kiremu, Limu, and Amuru districts in Western Ethiopia. All indices were estimated by using thermal bands and multispectral bands from Landsat TM 1990, Landsat ETM+ 2003, and Landsat OLI/TIRS 2020. The correlation of LST with NDVI, NDBaI and MNDWI were analyzed by using scatter plot. Accordingly, the NDBaI was positive correlation with LST (R^2 = 0.96). However, NDVI and MNDWI were substantially negative relationship with LST (R^2 = 0.99, 0.95), respectively. The result shows that, LST was increased by 5 °C due to decline of vegetation cover and increasing of bare land over the study periods. Finally, our result recommended that, decision-makers and environmental analysts should give attention on the importance of vegetation cover, water bodies and wetland in climate change mitigation, particularly, LST in the study area.

1. Introduction

The majority of human activities are the primary cause of the continuous loss of vegetation cover on the earth's surface (Sahana et al., 2016). The decrease in vegetation was a contributing factor to the increase in land surface temperature (LST). Song et al. (2021) highlights that vegetation is the main influencing factors that driven LST. The LST is one of the crucial indicators of ecological functioning of the environment. The LST is indicates the temperature of the Earth's skin, which is an important component in regional and global land surface processing studies (Thanh et al., 2018). The LST is increasing at global level due to land use land cover conversion (Moisa et al., 2022a). Studies conducted in different parts of Ethiopia confirmed that there is a substantial increasing trend of LST (Moisa et al., 2022b; Wolteji et al., 2022; Merga et al., 2022; Dissanayake et al., 2019). Similar to LST, the atmospheric temperature is significantly increasing as a results of land use land cover change (Gemeda et al., 2020; Gemeda et al., 2021; Gemeda et al., 2022; Moisa et al., 2022c).

To quantitatively describe degraded land, the Normalized Difference Barren Index (NDBaI) and the Modified Normalized Difference Water Index (MNDWI) were used (Gao, 1996; Zha et al., 2003). The LST were compared to the Normalized Difference Vegetation Index (NDVI), NDBaI, and MNDWI to provide ambient environmental condition for living things (Qinqin et al., 2012). Vegetation based indices can indicates the existence and abundancies of vegetation cover (Moisa et al., 2022a; Iang and Tian, 2010).

Analysis of spatial flexibility of the NDVI, LST, NDBaI, and MNDWI are tremendously crucial for decision making and natural resources monitoring in natural and environmental investigations (Zareie et al., 2016). In addition, NDVI has been used to confirm the importance for represent distribution of green space (Yuan and Bauer, 2007). Furthermore, several scholars raised that, remote sensing indices like NDVI

Abbreviations: LST, Land surface temperature; MIR, Middle infrared; MNDWI, Modified normalized difference water index; NDBaI, Normalized difference barren index; NDVI, Normalized difference vegetation index; NIR, Near infrared.

* Corresponding author.
E-mail address: mitikubadasa10@gmail.com (M.B. Moisa).

https://doi.org/10.1016/j.aiia.2022.06.002

and MNDWI were gradually declined due to forest fires, deforestation, expansion of urbanization, agricultural land expansion, and expansion of grazing land from which NDBaI, and LST were increased (Zhou and Wang, 2011; Mimbrero et al., 2014).

Although these indices have been used to model LST in previous study (Chen et al., 2006), only a few of them have compared index results from different years to monitor surface temperature. Even though, agricultural expansion is the main causes that aggravated climate change particularly LST in western parts of Ethiopia. No research has been conducted around Gida Kiremu, Limu, and Amuru district. It is obvious that the LST has increased over time due to a decline in vegetation cover for agricultural expansion. In addition, wetland degradation and the increment of barren land were other causes for the rising of LST. Therefore, this study attempted to analyze LST based on remote sensing indices such as NDVI, NDBaI, and MNDWI in western Ethiopia. This paper is organized as follows: the first section introduces the general introduction on LST and its correlation with different indices; Section two describes materials and methods which includes the study area descriptions, data types and sources, and method of data analysis; Section three presents' results and discussions and the final section concludes the findings of the study.

2. Materials and methods

2.1. Description of the study area

This study is conducted in East Wollega and Horo Guduru Wollega Zones and located between $9^0 27'00''$ and $10^0 18'00''$ N, and $36^0 19'30''$ and $37^0 10'30''$ E. Two districts namely: Gida Kiremu and Limu selected is located in East Wollega Zone while Amuru district is administratively located in the Horo Guduru Wollega Zone, Oromia National Regional State Western Ethiopia (Fig. 1). The study area elevation ranges from 713.32 to 2496.61 m above mean sea level. It has a total area of 5086.65km^2.

2.2. Climate

The average monthly rainfall of the current study area is ranged between 14.32 and 338 mm /year. The study area receive high rainfall during summer that starts in June and ends in September and short rain season is in, spring, which encompass March, April, and May.

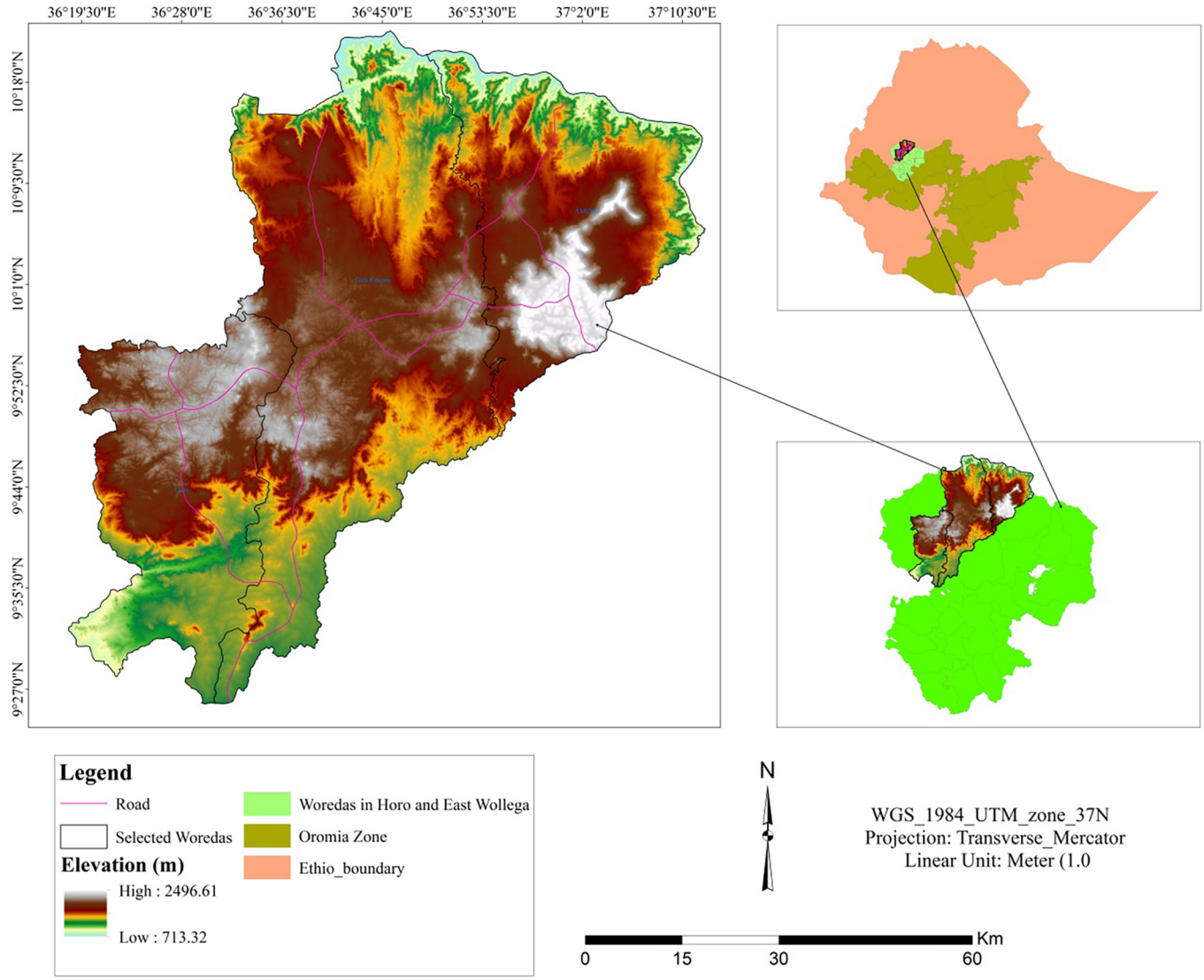

Fig. 1. Location map of the study area.

2.2.1. Soil types

Soil types of the study area were classified into sixteen in number namely: - calcic cambisols,calcic xerosols,chromic cambisols, chromic luvisols, dystric gleysols, dystric nitisols, eutric cambisols, eutric nitisols, gypsic yermosols, haplic xerosols, leptosols, orthic acrisols, orthic luvisols, orthic solonchaks, phaeozems, vertic cambisols from which dystric nitisols is the most dominants(2123.5 km^2) and least dominant soil type is phaeozems with an area of (2 km^2).

2.3. Socio economic activities

Mixed agriculture namely crop production and livestock production are the most popular income sources of smallholders farmers. From crop production, Maize, groundnut, niger seed, lentil, beans, and peas and some vegetables (potato, onions, garlic) and fruits like mango, papaya, oranges and bananas are mostly dominants agricultural products of the study areas. The agricultural activity of the study area is mainly depending on rain-fed.

2.4. Data types and sources

Landsat images from three years were used in this study. The USGS (http://earthexplorer.usgs.gov/) provides free downloads of the thermal and multispectral bands of Landsat TM 990, Landsat ETM+ 2003, and Landsat OLI/TIRS 2020. Detailed information regarding these data is presented in (Table 1). Software used for this study were, ArcGIS 10.3 version and ERDAS imagine 2015.

2.5. Method of data analysis

The LST, NDVI, MNDWI, and NDBaI were calculated in this study. The methodology flow diagram of the study was presented in (Fig. 2).

2.5.1. Normalized difference vegetation index (NDVI)

This index was used to calculate the amount of vegetation covering the earth's surface. The NDVI was estimated using multi-spectral bands from Landsat images collected over the course of the investigation. Band 4 was used to measure near-infrared bands on Landsat 5 and 7, and band 5 was used for Landsat 8. The red band of the Landsat data were measured using band 4 for Landsat 8 and band 3 for Landsat 5 and 7. The formula for this index is presented in (Eq. (1))

$$NDVI = \frac{NIR - R}{NIR + R} \tag{1}$$

The NDVI scale spans from −1.0 to 1.0. For healthy and dense vegetation, the NDVI values are always between 0.2 and 0.9 (Bustos and Meza, 2015). Vegetation such as rock, water, and barren plains, on the other hand, were represented by values less than 0.1 (Fu and Burgher, 2015).

2.5.2. Modified normalized difference water index (MNDWI)

When modelling the thermal environment, the MNDWI is assigned to represent water areas, which typically display notable variations in thermal characteristics (Xu, 2008; Zhifeng and Jianjun, 2012). The formula was developed using the green band (band 2 for landsat 5 and 7, band 3 for Landsat 8) and middle infrared (band 5 for Landsat 5 and 7, band 6 for landsat 8) reflectance values (Eq. (2)).

$$MNDWI = \frac{Green - MIR}{Green + MIR} \tag{2}$$

2.5.3. Normalized difference barren index (NDBaI)

When estimating the thermal environment, NDBaI was chosen to represent barren terrain areas, which often show large variances in thermal characteristics (Zhifeng and Jianjun, 2012). It is estimated using the reflectance of medium infrared (band 5 for Landsat 5 and 7, band 6 for Landsat 8) and thermal infrared (band 6 for Landsat 5 and 7, band 10 and 11 for Landsat 8) satellites (Eq. (3)).

$$NDBaI = \frac{MIR - TIR}{MIR + TIR} \tag{3}$$

2.5.4. Retrieval of land surface temperature (LST)

The mono-window algorithm (Qin et al., 2001), single channel, was created from Landsat TM, ETM+, and OLI/TIRS data (Jiménez-Muñoz and Sobrino, 2003). LST was extracted from Landsat 8 data with one bands using mono window method from band 10. LST is determined by employing the brightness temperature of the two bands of Thermal Infrared (TIR), as well as the mean and difference in land surface emissivity (Cheng et al., 2015).

2.5.4.1. Step I: Conversion of DN in to radiance.

A. Mono window algorithm

Before calculating the brightness temperature, the mono window technique converted the digital data into an at-sensor radiance sensor.

The TM and ETM+ DN value ranges between 0 and 255 (Eq. (4)).

$$L\lambda = \frac{LMAX\lambda - LMIN\lambda}{QCALMAX - QCALMIN} x\,(DN - QCALMIN) + LMIN\lambda \tag{4}$$

where:

QCLA = quantized calibrated pixel value in Digital Number (DN).

LMINλ = spectral radiance scaled to QCALMIN in watts/(meter squared*ster* μm).

LMAXλ = spectral radiance scaled to QCALMAX in watts/(meter squared*ster* μm).

QCALMIN = minimum quantized calibrated pixel value corresponding to LMINλ in DN.

QCALMAX = maximum quantized calibrated pixel value corresponding to LMAXλ in DN = 255.

For Landsat 8, the mono window algorithm (MWA) was also applied to estimate the LST as used by other experts (Aik et al., 2020; Sahana et al., 2016; Atitar and Sobrino, 2009). The Landsat 8 TIRS Digital Numbers (DNs) for band 10 were first converted into spectral radiance (Eq. (5)).

$$L\lambda = (ML{*}QCal) + AL \tag{5}$$

where;

$L\lambda$ is Top of Atmosphere (TOA) spectral radiance (Wm^{-2} sr^{-1} μm^{-1}).

ML is Band-specific multiplicative rescaling factor from the metadata (RADIANCE_MULT_BAND x, where x is number of bands).

AL is a band-specific additive rescaling factor from the metadata (RADIANCE_ADD_BAND_x, where x is the band number).

QCal is quantized and calibrated standard product pixel values (DN).

2.5.4.2. Step II. Conversion to temperature (ETM+). Based on land surface emissivity, atmospheric trans-emissivity, brightness temperature, and

Table 1
Remote sensing data used for the study.

Satellite Image	Path/Row	Sensor	Resolution (m)	No of bands	Date of Acquisitions
Landsat 5	170/53	TM	30	7	12-01-1990
Landsat 7	170/53	ETM+	30	7	20-02-2003
Landsat 8	170/53	OLI/TIRS	30	11	11-02-2020

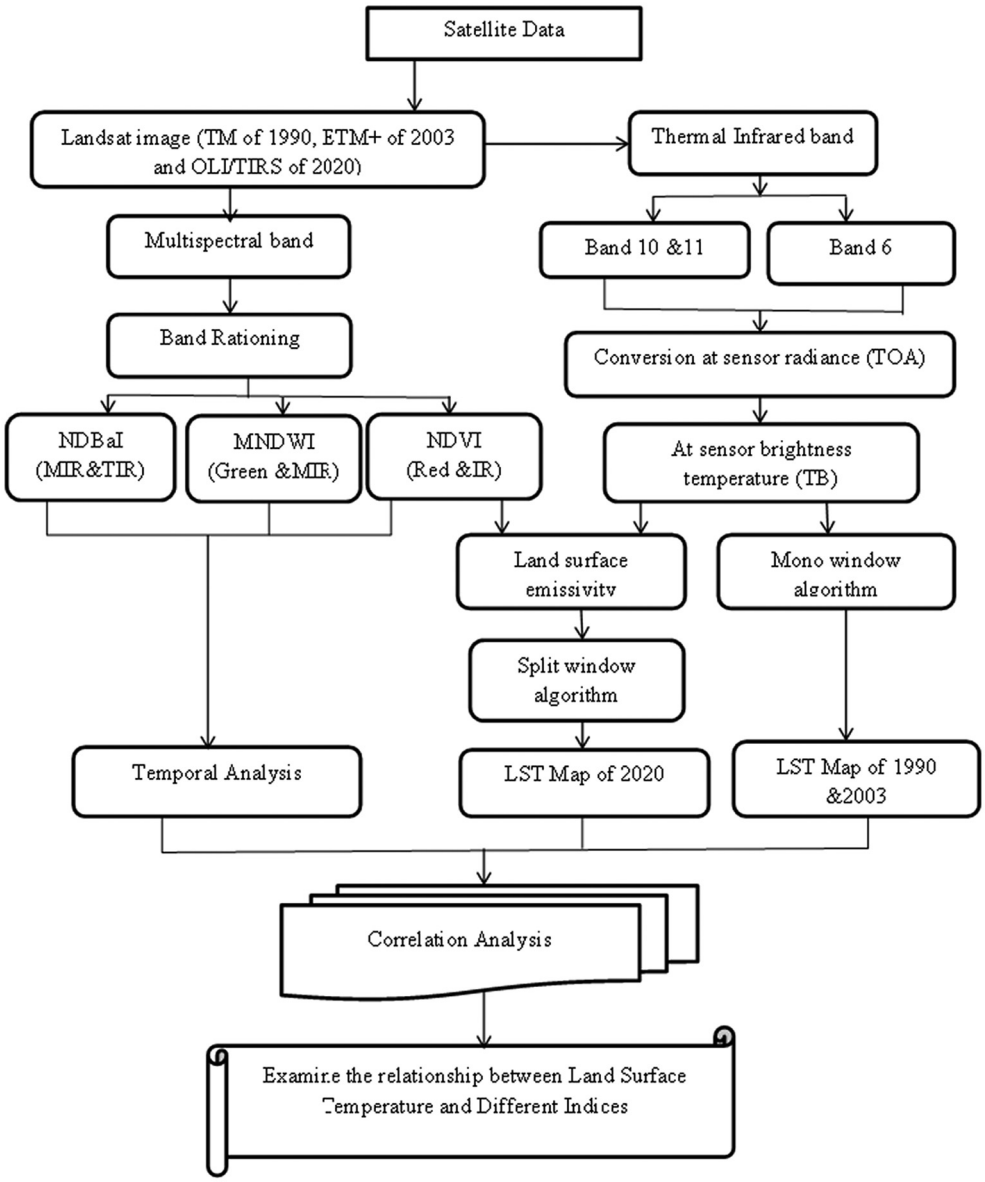

Fig. 2. Methodological flowchart of the study.

average atmospheric temperature, the mono-window algorithm was used to determine the LST (Zhang et al., 2006). The spectral radiance (as mentioned above) of TM and ETM+ Band 6 imaging can also be transformed into a more physically usable quantity (Eq. (6)). The conversion formula is as follows:

$$T = \frac{K2}{ln\left(\frac{K1}{L\lambda} + 1\right)} \tag{6}$$

where T = Effective at-satellite temperature in Kelvin.

K2 = Calibration constant 2.

K1 = Calibration constant 1.

Lλ = Spectral radiance in watts/(meter squared * ster * μm).

For this investigation, mono window algorithm (MW) was also used to calculate LST in landsat 8. It calculates mean land surface emissivity and then to estimates the brightness temperatures from band 10 of landsat 8.

TB10 is brightness temperature of band 10 (Kelvin K);

Ɛ is mean value of Land Surface Emissivity (LSE) of TIR bands;

W is content of water vapors in the atmosphere;

Ɛ is LSE of band 10 to estimate LST (Eq. (7)):

$$BT = \frac{K2}{\ln\left(\frac{K1}{L\lambda} + 1\right)} \tag{7}$$

where;

BT: is effective at-sensor brightness temperature (K);

K2: is calibration constant 2 (K);

K1: is calibration constant 1 (W/ (m^2 * sr * μm));

Lλ: is spectral radiance at the sensor's aperture (W/ (m^2 * sr * μm)); and.

Ln: is natural logarithm.

2.5.4.3. Step III: Land surface emissivity estimation. According to Sobrino et al. (2004), the emissivity is calculated using (Eq. (9))

$$\varepsilon = 0.004 * PV + 0.986 \tag{8}$$

where PV is the vegetation proportion obtained according to.

Carlson and Ripley formula (10);

$$PV = \left[\frac{NDVI - NDVImin}{NDVImax - NDVImin}\right]^2 \quad (9)$$

The calculated radiant surface temperatures will be corrected for emissivity using the equation (Eq. (11)):

$$LST = \frac{TB}{1 + (\lambda \frac{TB}{P}) In\varepsilon} \quad (10)$$

where;

LST: land surface temperature (in Kelvin);

TB: radiant surface temperature (in Kelvin).

λ: the wavelength of emitted radiance (10.8 μm), and Inε is emissivity.

ρ: $h \times c/\sigma (1.438 \times 10^{-2}$ mK); h is Planck's constant (6.26×10^{-34} J s); c is the velocity of light (2.998×10^{8} m/s); σ is Stefan Boltzmann's constant (1.38×10^{-23} J K^{-1}); and ε is land surface emissivity.

Finally, the findings of Landsat TM, ETM+ and OLI/TIRS LST measurements were converted to degrees Celsius by subtracting 273.15. (Eq. (11)) was used to convert temperature in degrees Kelvin (K) to degrees Celsius (°C).

$$0C = K - 273.15 \quad (11)$$

where: °C = LST result in degree Celsius;

K = LST result in degree Kelvin.

3. Result and discussion

3.1. Analysis of land surface temperature

The spatial pattern of LST in the study area was determined for the years 1990, 2003, and 2020, respectively. In all of the years studied, the northeastern and southwestern parts of the study area had high LST (Fig. 3). The increasing of LST in the study area is associated with the declining of vegetation cover and increasing of bare land.

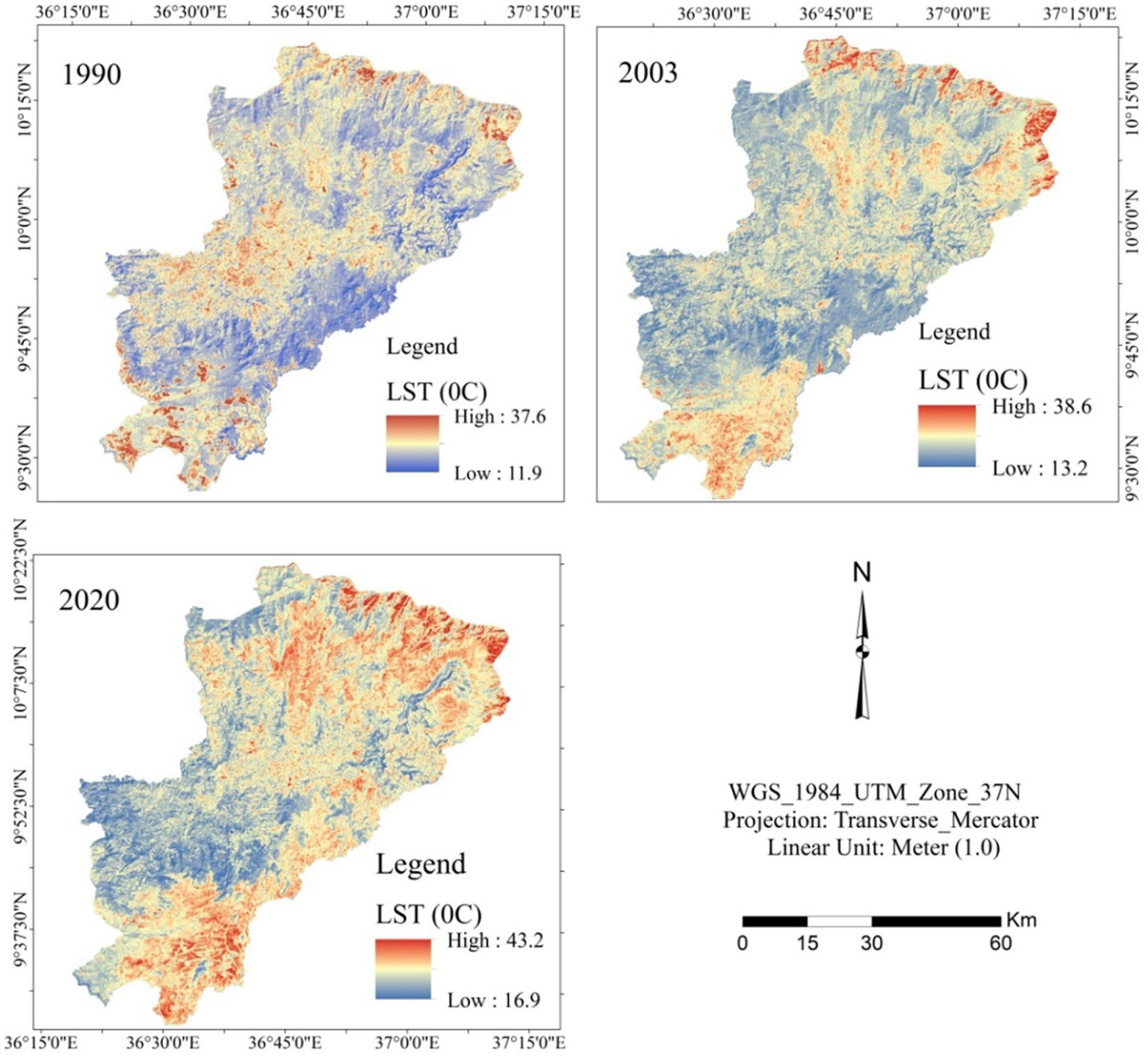

Fig. 3. LST map of the study area.

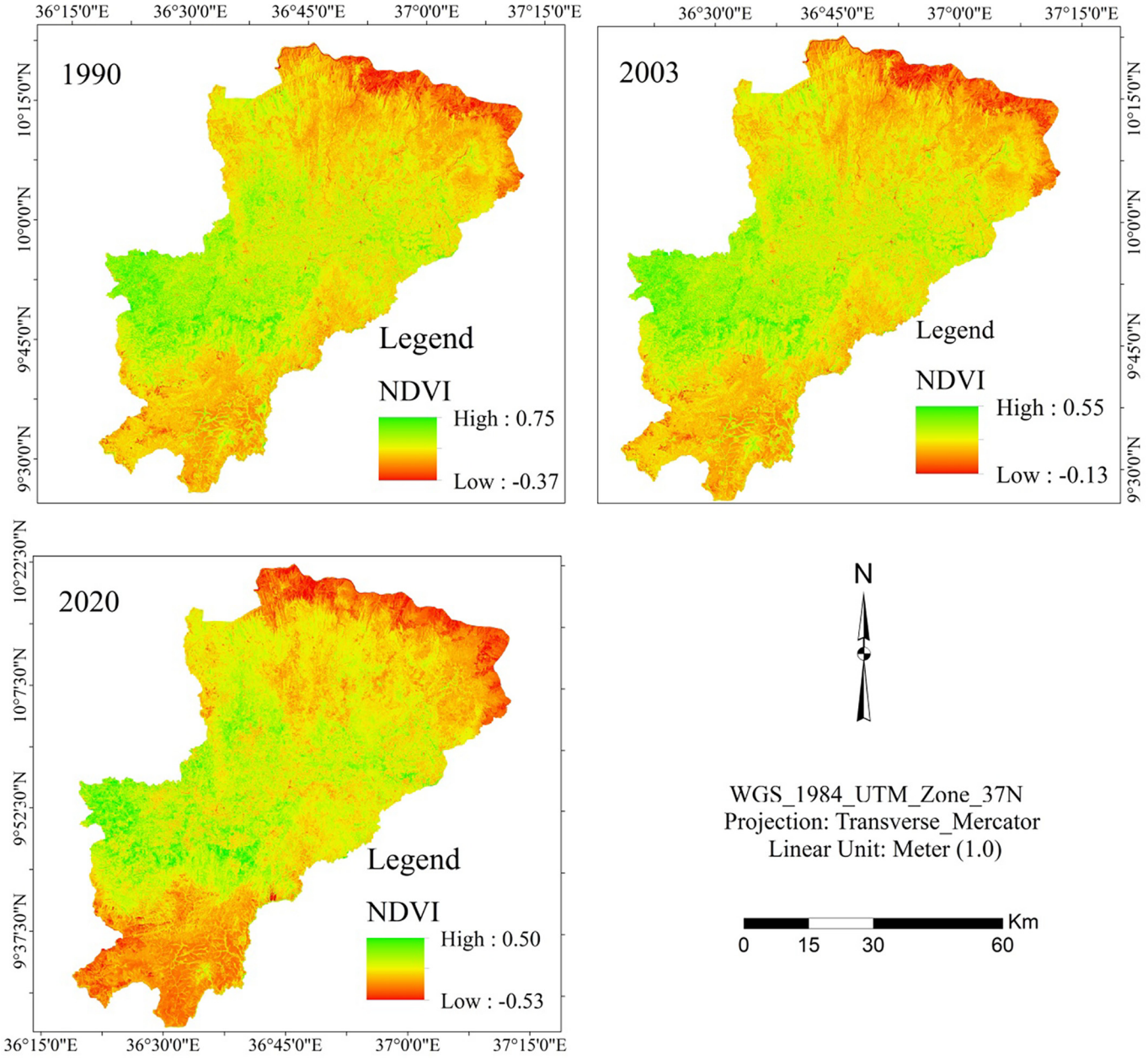

Fig. 4. Normalized Difference Vegetation Index map of the study area.

Due to the existance of substantial vegetation cover, the eastern, central, and western parts of the research region experienced relatively low LST.

The mean LST gradually increased from 23.70 °C in 1990 to 24.30 °C in 2003 to 28.70 °C in 2020. From 1990 to 2020, an average temperature was increased by 5 °C. Comparable result has been reported by Moisa et al., 2022a, which found an increment of LST by 5.6 °C in Anger River Sub-basin between the year 1991, and 2020. As compared to 1990, and 2003, the year 2020 is the most extreme temperature. The increasing trend of LST is associated with the declining of vegetation cover and

Table 2
Correlation between LST, NDVI, NDBaI and MNDWI.

Correlation	*LST*	*NDBaI*	*NDVI*	*MNDWI*
LST	1			
NDBaI	0.95767*	1		
NDVI	−0.9995*	−0.9627*	1	
MNDWI	−0.9581*	−0.979*	0.98452*	1

* shows that Correlation values between them.

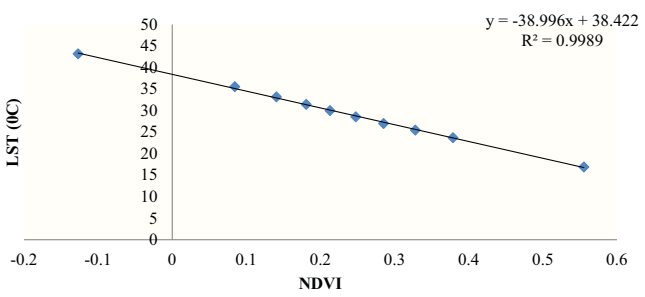

Fig. 5. Relationship of LST and NDVI of study area.

wetland degradation driven by expansion of agricultural land. The LST is expected to increase due to global warming. For instance, Rasul et al. (2012) predict that by 21 century, the temperature will have increased by 1.40 °C to 5.80 °C during the twentieth century which confirmed the present study.

3.2. Correlation between LST and NDVI

LST values were discovered to range from maximum temperature (43.2 °C) to minimum temperature (16.9 °C), whereas NDVI values are found to range from 0.50 to −0.53 maximum to minimum. The results show that LST and NDVI have a strong negative correlation (R^2 = 0.99). Wolteji et al. (2022) found a moderate negative relationship between NDVI and LST over the Rift Valley Region of Ethiopia. It shows that high LST are more closely related to low vegetation cover and vice versa. The distribution of NDVI over the study period is presented in (Fig. 4). The relationship between the two factors (LST and NDVI) in 2020 is shown in (Table 2 and Fig. 5). This result of study is in line with (Alemu, 2019; Wedajo et al., 2019; Merga et al., 2022) they confirmed that, LST was increased as decline of vegetation cover and both of them had strong negative relationship.

3.3. Correlation between LST and NDBaI

Barren land of the study area is increasing due to agricultural expansion and decline of vegetation cover. The results demonstrate a substantial positive correlation between LST and NDBaI (R^2 = 0.96). It demonstrates that high LST can be found on degraded or barren terrain with a high NDBaI value (Fig. 6). The relationship between two parameters was shown in (Fig. 7). The result of the study more consistency with the result of (Zhifeng and Jianjun, 2012) and they stated that barren land was substantial positive correlation with LST.

3.4. Correlation between LST and MNDWI

Vegetation water content (wetland) was decreased due to decline of vegetation and increasing of LST. Expansion of agricultural

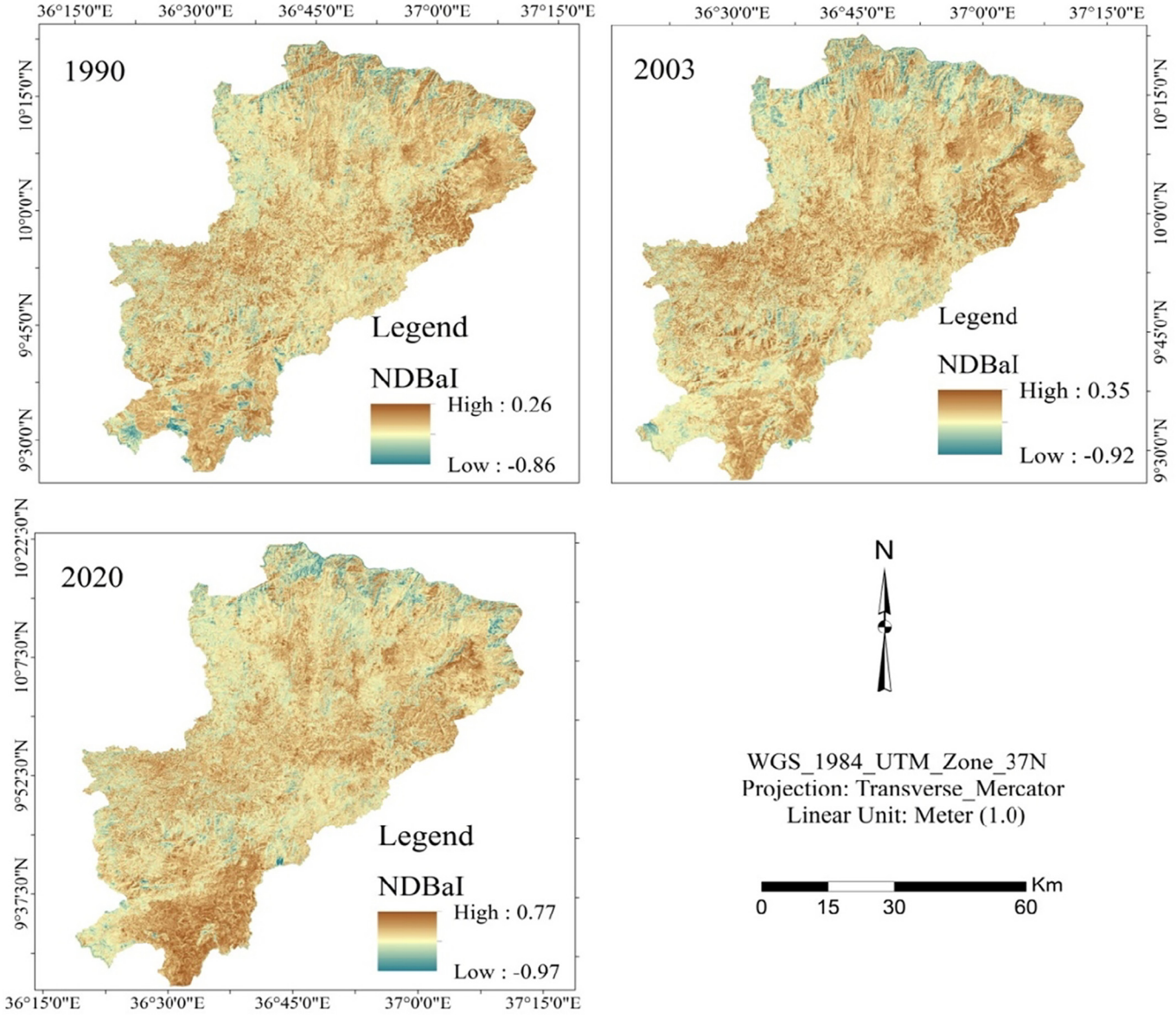

Fig. 6. Normalized Difference Barren Index (NDBaI) map of the study area.

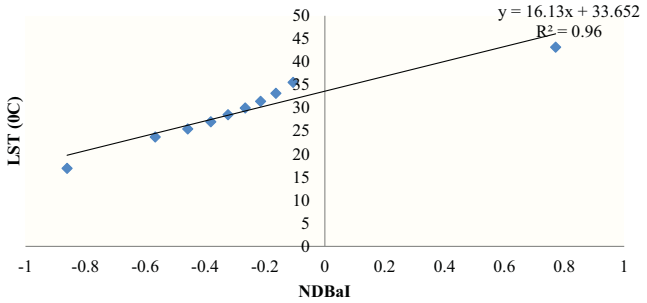

Fig. 7. Relationship of LST and NDBaI of study area.

land and increasing of barren land which together increase LST was the main factors for decreasing of MNDWI in the study area. The results shows that a negative strong association between LST and MNDWI, with coefficient determination of (R2 = 0.95). MNDWI is high in the northern and southern parts of the study area (Fig. 8). The findings reveal that high LST are more commonly recorded in low-water locations. The relationship between LST and MNDWI was presented in (Fig. 9). The result is agreed with the result of previous studies (Zhou and Wang, 2011; Zhifeng and Jianjun, 2012). The relationship between LST and other indices were reported in (Table 2). The NDBaI has a direct association with LST, while NDVI and MNDWI have an inverse relationship with LST.

3.5. Correlation between LST and Time of study

The mean LST of the study area was correlated the study period. The result shows that mean of LST was positive relationship with time of study with $R^2 = 0.89$. As time increased mean of LST was increased (Fig. 10).

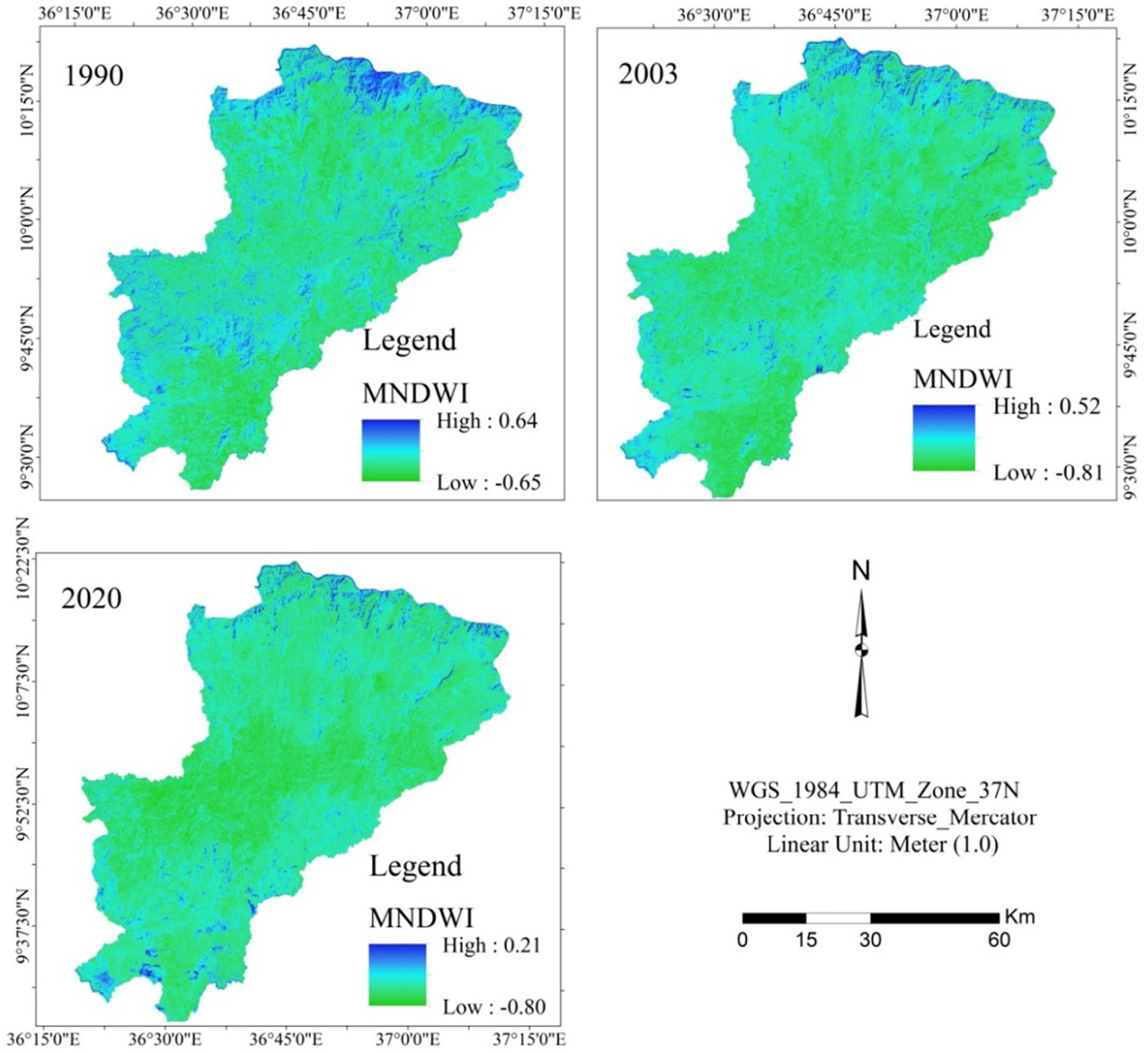

Fig. 8. Modified Normalized Difference Water Index (MNDWI) map of the study area.

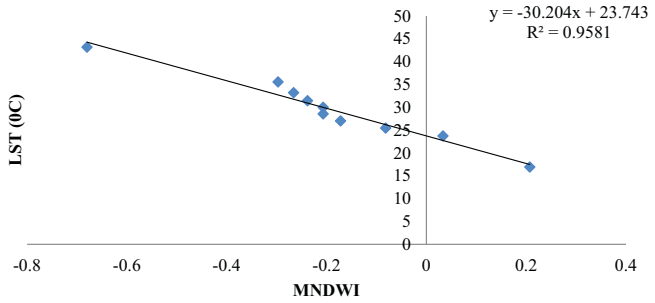

Fig. 9. Relationship of LST and MNDWI of study area.

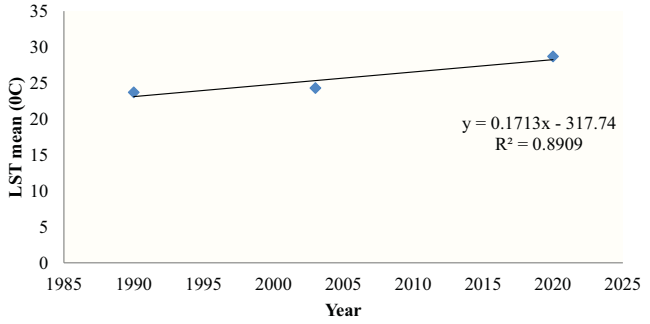

Fig. 10. Relationship of LST with year of study.

4. Conclusions

In this article, we use remote sensing data to assess the spatial-temporal LST in relation to NDVI, NDBaI, and MNDWI indices in three districts of western Ethiopia: Gida Kiremu, Limu, and Amuru. Between 1990 and 2020, the temperature of the earth's surface increased by 5 °C. Our results concluded that the NDVI and MNDWI have a substantial negative relationship with LST, whereas NDBaI has a positive correlation with LST. Expansion of agricultural land is the main cause for decline of vegetation cover in the study area. Decline of vegetation cover is the cause for decrement of vegetation water content (wetland) and increasing of barren land. Moreover, LST is increasing over time and expanded to all directions in study area. Based on our findings, this study recommended the community awareness creation to promote the wise use of natural resources for its sustainability. In addition, further studies on the impacts of LST agricultural production can enhance our understanding of the impacts of environmental changes on community livelihhoods.

Consent for publication

The authors agreed to publish the manuscript on Artificial Intelligence in Agriculture.

Availability of data

Available in this manuscript.

Funding

No funding received for this research.

Author contributions

MBM involved in research design, data collection, data analysis, and draft manuscript writing. LBH and END involved in data analysis. DOG and BTG participated in methodology, data analysis and manuscript edition. All authors read and approved the final manuscript.

CRediT authorship contribution statement

Mitiku Badasa Moisa: Conceptualization, Data curation, Formal analysis, Investigation, Methodology, Resources, Software, Validation, Visualization, Writing – original draft, Writing – review & editing. **Bacha Temesgen Gabissa:** Formal analysis, Investigation, Methodology, Resources, Writing – review & editing. **Lachisa Busha Hinkosa:** Formal analysis, Investigation, Methodology, Resources, Writing – review & editing. **Indale Niguse Dejene:** Formal analysis, Investigation, Methodology, Resources, Writing – review & editing. **Dessalegn Obsi Gemeda:** Formal analysis, Investigation, Methodology, Resources, Writing – review & editing.

Declaration of Competing Interest

The authors declared no competing interest.

Acknowledgments

The authors would like to acknowledge Wollega University Shambu Campus Faculty of Technology, Faculty of Agriculture, Wollega University Nekemte campus College of Natural and computational sciences and Jimma University College of Agriculture and Veterinary Medicine for the existing facilities to conduct this study.

References

Aik, D.H.J., Ismail, M.H., Muharam, F.M., 2020. Land use/land cover changes and the relationship with land surface temperature using Landsat and MODIS imageries in Cameron Highlands, Malaysia. Land 9, 372.

Alemu, M.M., 2019. Analysis of Spatio-temporal land surface temperature and normalized difference vegetation index changes in the Andassa watershed, Blue Nile Basin, Ethiopia. J. Resour. Ecol. 10 (1), 77–85.

Atitar, M., Sobrino, J., 2009. A split-window algorithm for estimating LST from meteosat 9 data: test and comparision with data and MODIS LSTs. IEEE Geosci. Remote Sens. Lett. 6, 122–126.

Bustos, E., Meza, F.J., 2015. A method to estimate maximum and minimum air temperature using MODIS surface temperature and vegetation data: application to the Maipo Basin, Chile. Theor. Appl. Climatol. 120 (1–2), 211–226. https://doi.org/10.1007/s00704-014- 1167-2.

Chen, X., Zhao, H., Li, P., Yin, Z., 2006. Remote sensing image-based analysis of the relationship between urban heat island and land use/cover changes. Remote Sens. Environ. 104, 133–146.

Cheng, X., Wei, B., Chen, G., Song, C., 2015. Influence of park size and its surrounding urban landscape patterns on the park cooling effect. J. Urban Plan. Dev. 141, A4014002.

Dissanayake, D., Morimoto, T., Murayama, Y., Ranagalage, M., 2019. Impact of landscape structure on the variation of land surface temperature in sub-Saharan region: a case study of Addis Ababa using Landsat data (1986–2016). Sustainability 11, 2257. https://doi.org/10.3390/su11082257.

Fu, B., Burgher, I., 2015. Riparian vegetation NDVI dynamics and its relationship with climate, surface water and groundwater. J. Arid Environ. 113, 59–68. https://doi.org/10.1016/j.jaridenv.2014. 09.010.

Gao, B.C., 1996. NDWI a normalized difference water index for remote sensing of vegetation liquid water from space. Remote Sens. Environ. 58, 257–266.

Gemeda, D.O., Feyssa, D.H., Garedew, W., 2020. Meteorological data trend analysis and local community perception towards climate change: a case study of Jimma City, southwestern Ethiopia. Environ. Dev. Sustain. 23, 5885–5903.

Gemeda, D.O., Korecha, D., Garedew, W., 2021. Evidences of climate change presences in the wettest parts of southwest Ethiopia. Heliyon 7 (9), e08009. https://doi.org/10.1016/j.heliyon.2021.e08009.

Gemeda, D.O., Korecha, D., Garedew, W., 2022. Monitoring climate extremes using standardized evapotranspiration index and future projection of rainfall and temperature in the wettest parts of Southwest Ethiopia. Environ. Challenges 7, 100517. https://doi.org/10.1016/j.envc.2022.100517.

Iang, J., Tian, G., 2010. Analysis of the impact of land use/ land cover change on land surface temperature with remote sensing. Procedia Environ. Sci. 2, 571–575.

Jiménez-Muñoz, C., Sobrino, J., 2003. A generalized single-channel method for retrieving land surface temperature from remote sensing data. J. Geophys. Res. 108.

Merga, B.B., Moisa, M.B., Negash, D.A., Ahmed, Z., Gemeda, D.O., 2022. Land surface temperature variation in response to land-use and land-cover dynamics: a case of Didessa River sub-basin in Western Ethiopia. Earth Syst. Environ. https://doi.org/10.1007/s41748-022-00303-3.

Mimbrero, M.R., Vlassova, L., Pé, F., 2014. Analysis of the relationship between land surface temperature and wildfire severity in a series of landsat images. Remote Sens. 6, 6136–6162. https://doi.org/10.3390/rs6076136.

Moisa, M.B., Dejene, I.N., Merga, B.B., Gemeda, D.O., 2022a. Impacts of land use/land cover dynamics on land surface temperature using geospatial techniques in Anger River sub-basin, Western Ethiopia. Environ. Earth Sci. 81, 99. https://doi.org/10.1007/s12665-022-10221-2.

Moisa, M.B., Merga, B.B., Gemeda, D.O., 2022b. Multiple indices-based assessment of agricultural drought: a case in Gilgel gibe sub-basin, Southern Ethiopia. Theor. Appl. Climatol. 148, 455–464.

Moisa, M.B., Merga, B.B., Gemeda, D.O., 2022c. Urban heat island dynamics in response to land use land cover change: a case of Jimma city, southwestern Ethiopia. Theor. Appl. Climatol. https://doi.org/10.1007/s00704-022-04055-y.

Qin, Z., Karnieli, A., Berliner, P., 2001. A mono-window algorithm for retrieving land surface temperature from Landsat TM data and its application to the Israel-Egypt border region. Int. J. Remote Sens. 21, 3719–3746.

Qinqin, Sun, Zhifeng, Wu., Jianjun, Tan, 2012. The relationship between land surface temperature and land use/land cover in Guangzhou, China. Environ. Earth Sci. 65, 1687–1694. https://doi.org/10.1007/s12665-011-1145-2.

Rasul, G., Mahmood, A., Sadiq, A., Khan, S.I., 2012. Vulnerability of the Indus Delta to climate change in Pakistan. Pakistan J. Meteorol. 2012, 8(16).

Sahana, M., Ahmed, R., Sajjad, H., 2016. Analyzing land surface temperature distribution in response to land use/land cover change using split window algorithm and spectral radiance model in Sundarban biosphere reserve, India. Model. Earth Syst. Environ. 2, 81. https://doi.org/10.1007/s40808-016-0135-5.

Sobrino, J.A., Jimenez-Munoz, J.C., Paolini, L., 2004. Land surface temperature retrieval from LANDSAT TM5. Remote Sens. Environ. 90, 434–440.

Song, Z., Yang, H., Huang, X., Yu, W., Huang, J., Ma, M., 2021. The spatiotemporal pattern and influencing factors of land surface temperature change in China from 2003 to 2019. Int. J. Appl. Earth Obs. Geoinf. 104 (2021), 102537. https://doi.org/10.1016/j.jag.2021.102537.

Thanh, Noi Phan, Martin, Kappas, Trong, Phuong, 2018. Land surface temperature variation due to changes in elevation in Northwest Vietnam. Climate 6, 28. https://doi.org/10.3390/cli6020028.

Wedajo, G.B., Muleta, M.K., Gessesse, B., Koriche, S.A., 2019. Spatiotemporal climate and vegetation greenness changes and their nexus for Dhidhessa River basin, Ethiopia. Environ. Syst. Res. 8, 31. https://doi.org/10.1186/s40068-019-0159-8.

Wolteji, B.N., Bedhadha, S.T., Gebre, S.L., Alemayehu, E., Gemeda, D.O., 2022. Multiple indices based agricultural drought assessment in the Rift Valley region of Ethiopia. Environ. Challenges 7, 100488.

Xu, H., 2008. A new index for delineating built-up land features in satellite imagery. Int. J. Remote Sens. 29, 4269–4276.

Yuan, F., Bauer, M.E., 2007. Comparison of impervious surface area and normalized difference vegetation index as indicators of surface urban heat island effects in Landsat imagery. Remote Sens. Environ. 106, 375–386.

Zareie, S., Khosravi, H., Nasiri, A., 2016. Using Landsat thematic mapper (TM) sensor to detect change in land surface temperature in relation to land use change in Yazd, Iran. Solid Earth 7, 1551–1564. https://doi.org/10.5194/se-7-1551-2016.

Zha, Y., Gao, J., Ni, S., 2003. Use of normalized difference built-up index in automatically mapping urban areas from TM imagery. Int. J. Remote Sens. 24, 583–594.

Zhang, Y., Yu, T., Gu, X., Zhang, Y., Chen, L., 2006. Land surface temperature retrieval from CBERS-02 IRMSS thermal infrared data and its applications in quantitative analysis of urban heat islands effects. J. Remote Sens. Beijing 10, 789.

Zhifeng, W.U., Jianjun, Jim Tan, 2012. The relationship between land surface temperature and land use/land cover in Guangzhou, China. Environ. Earth Sci. 65, 1687–1694. https://doi.org/10.1007/s12665-011-1145-2.

Zhou, Xiaolu, Wang, Yi-Chen, 2011. Dynamics of land surface temperature in response to land-use/cover change. Geogr. Res. 49 (1), 23–36. https://doi.org/10.1111/j.1745-5871.2010.00686.x.